

Electronic structure and magnetic properties of the spin-1/2 Heisenberg magnet Bi_2CuO_4

O. Janson,^{1,2} R. O. Kuzian,³ S.-L. Drechsler,⁴ and H. Rosner^{1,*}

¹Max-Planck Institut für Chemische Physik fester Stoffe, Nöthnitzer Strasse 40, D-01187 Dresden, Germany

²St. Petersburg State University, Universitetskaya naberezhnaya 7/9, 199034 St. Petersburg, Russia

³Institute for Problems of Materials Science Krzhizhanovskogo 3, 03180 Kiev, Ukraine

⁴Leibniz-Institut für Festkörper- und Werkstoffforschung Dresden, P.O. Box 270116, D-01171 Dresden, Germany

(Received 27 September 2006; revised manuscript received 20 July 2007; published 18 September 2007)

The electronic and magnetic structure of the spin-1/2 magnet Bi_2CuO_4 is investigated by band structure calculations within the local (spin) density approximation [L(S)DA]. The insulating compound shows a complex of narrow, half-filled antibonding bands within the LDA, indicating the importance of strong on-site correlation effects. To describe the lowest-lying excitations, the strong Coulomb correlations have been taken into account by a subsequent mapping of the LDA band structure onto a tight-binding model and via an extended Hubbard model onto an extended Heisenberg model. Alternatively, the leading exchange interactions have been estimated applying the LSDA+ U method for different spin configurations in magnetic supercells. Using our estimated exchange constants, we calculated the spin wave dispersion and the Néel temperature within the random phase approximation. The calculated properties are in good agreement with experimental data, suggesting that the magnetic ground state of Bi_2CuO_4 is governed by the antiferromagnetic interaction between the structural one-dimensional cuprate chains.

DOI: 10.1103/PhysRevB.76.115119

PACS number(s): 74.72.Hs

I. INTRODUCTION

The influence of dimensionality and lattice geometry on the electronic and magnetic structure of crystalline compounds is a classical topic in solid state physics. Specifically, linear chains of exchange coupled spin-1/2 systems have always been the subject of extensive theoretical and experimental studies.^{1–7} Recently, the interest in quasi-one-dimensional magnets has been strongly increased because new unusual ground states resulting from the competition of ferromagnetic and antiferromagnetic interactions have been found. This competition arises from a ferromagnetic nearest neighbor exchange J_1 and an antiferromagnetic next nearest neighbor exchange J_2 . The resulting magnetic frustration with a frustration ratio $\alpha \sim J_2/J_1$ drives a helical magnetic order in the compounds LiVCuO_4 ($\alpha \sim -1.43$),⁸ NaCu_2O_2 ($\alpha \sim -2$),^{9,10} and LiCu_2O_2 ($\alpha \sim -1$).^{11–14} Applying a magnetic field, the latter system shows even ferroelectric properties in the spiral state.¹⁵ Slight modifications of the chain geometry in $\text{Li}_2\text{ZrCuO}_4$ lead to a strongly changed frustration ratio $\alpha \sim 1/4$, placing this system close to the ferromagnetic quantum critical point.¹⁶ These examples show that the magnetic ground state is strongly entangled with the arrangement of the magnetic units in such low-dimensional systems.

Originally, Bi_2CuO_4 was described as a quasi-one-dimensional spin-1/2 compound containing ferromagnetically ordered chains that are antiferromagnetically coupled.¹⁷ This seems to be very similar to the situation in Li_2CuO_2 , where ferromagnetic chains result from a competition of first- and second-neighbor coupling along edge-shared CuO_2 chains.^{18–22} On the other hand, structural peculiarities and Raman and neutron scattering data strongly favor a three-dimensional nature of the magnetic coupling in Bi_2CuO_4 . This is supported by the rather large ordered magnetic moment for a low-dimensional spin-1/2 compound reported between $0.7\mu_B$ in Ref. 23 and $0.93\mu_B$ in Ref. 24 together with

a Néel temperature of ≈ 45 K in Refs. 25 and 26 of the order of the leading exchange constant. However, despite many experimental studies of the electronic and magnetic structure of Bi_2CuO_4 (Refs. 23 and 27–30), the discussion is far from being settled. In particular, the values of the exchange parameters as well as the size and direction of the magnetic moment are still under debate. Therefore, we attempt to investigate the electronic and magnetic interactions by means of electronic structure calculations as an independent approach. Similar band structure studies, combining density functional investigations and model calculations, have provided deep and reliable insight into the nature of the magnetic ground state of many unusual spin-1/2 compounds.^{31–34}

The paper is organized as follows: In Sec. II, crystal and magnetic structures of Bi_2CuO_4 are briefly discussed. After a short description of the computational method in Sec. III, the results of the electronic structure calculation are presented and discussed in Sec. IV. The calculation of the spin wave dispersion and the Néel temperature is presented in Sec. V. Technical details of the tight-binding mapping and the analysis of the spin wave dispersion are given in Appendices A and B, respectively.

II. CRYSTAL STRUCTURE

The tetragonal crystal structure of Bi_2CuO_4 (Fig. 1) consists of isolated CuO_4^{6-} plaquettes, which are staggered in chains along the z axis. The neighboring in-chain plaquettes are twisted with respect to each other with a twist angle of about 33° . The chains are connected by BiO_4 units. The crystal structure was originally determined in the space group $I4$ in Ref. 35; later, the space group $P4/ncc$ proposed in Ref. 36 appeared to be more correct.^{24,25,37,38} For our electronic structure calculations, we used the crystallographic data obtained by neutron powder diffraction at 1.5 K (with the lat-

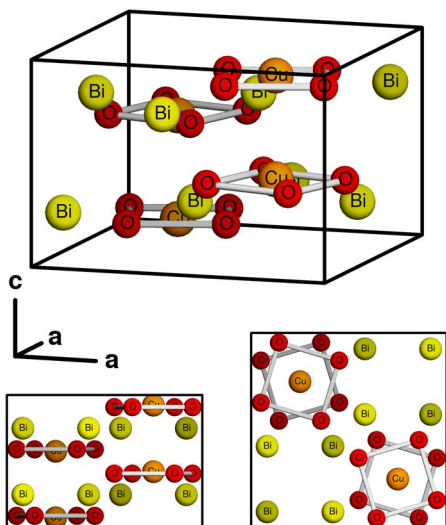


FIG. 1. (Color online) The crystal structure of Bi_2CuO_4 : perspective view (top), front view (down left), and lateral view (down right). The oxygen-oxygen bonds are shown only for the visualization of CuO_4 plaquettes. The chains of isolated plaquettes are stacked along z (top) in a staggered manner.

tice constants $a=8.4989 \text{ \AA}$ and $c=5.7973 \text{ \AA}$.²⁴

The magnetic structure of Bi_2CuO_4 consists of formally ferromagnetic chains along the tetragonal z axis that are antiferromagnetically ordered with respect to each other.^{24,25,37–40} The magnetic space group $P4/n'c'c'$, which was used for the description of this compound, is incorrect from our point of view; the magnetic group which allows the in-chain ferromagnetic order⁴¹ is $P4/n'cc$ according to Ref. 42. This magnetic structure can be described with two ferromagnetic sublattices that are shifted against each other on $(\frac{1}{2}a, \frac{1}{2}a, \Delta c)$ and are antiferromagnetic with respect to each other.

III. COMPUTATIONAL METHOD

A full-potential nonorthogonal local-orbital scheme (FPLO 5.00-18)⁴³ within the local (spin) density approximation [L(S)DA] was applied for the band structure calculations. In these scalar relativistic calculations, the Perdew and Wang parametrization of the exchange correlation potential⁴⁴ was chosen. The spin-orbit coupling was included for the calculations of the magnetic anisotropy. The L(S)DA+ U method⁴⁵ was used to take the strong on-site Coulomb correlations at the Cu site into account.

The following basis set was used: Bi ($4f5s5p5d$)/($6s6p6d$), Cu ($3s3p$)/($4s4p$) $3d$, and O ($2s2p3d$) [notation: (*semicore states*/*valence states*) polarization states]. All lower-lying states were treated as core states. The inclusion of semicore states was forced by their non-negligible overlap due to the large extension of their wave functions. The formally unoccupied Bi $6d$ and O $3d$ states were included to improve the completeness of the basis set.

The extension of the basis orbitals is controlled by an additional confining potential $\sim(r/r_0)^4$ and gets optimized

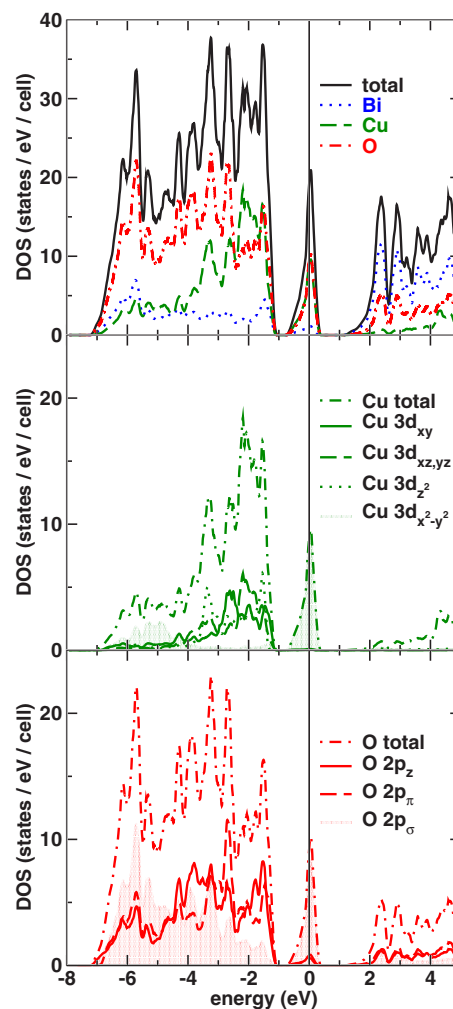


FIG. 2. (Color online) The LDA electronic density of states: total and site-resolved partial density of states (top) and orbital-resolved density of states for Cu $3d$ states (middle) and O $2p$ states (bottom). The Fermi level is at zero energy. Note the different scaling in the panels showing site-resolved and orbital-resolved densities of states.

with respect to the total energy. A k mesh of 490 points in the full Brillouin zone (60 points in the irreducible wedge) was used for the self-consistent calculations.

IV. RESULTS AND DISCUSSION

Figure 2 shows the electronic density of states of the non-magnetic LDA calculations yielding a valence band complex with a total band width of about 8 eV, typical for cuprates. The large energy difference between the bonding Cu-O states centered at -6 eV and the antibonding Cu-O states at Fermi level points to the strong covalency of Cu-O plaquette bond. The main contribution to the valence band originates from Cu $3d$ and O $2p$ states.

In Bi_2CuO_4 , Cu is formally in a $3d^9$ configuration; therefore, strong Coulomb correlations are expected which explain the experimentally observed²⁹ insulating behavior. It is well known that the LDA strongly underestimates these correlations, resulting in an incorrect metallic ground state. The

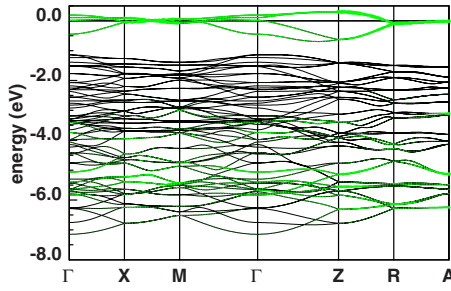


FIG. 3. (Color online) The band structure (black lines) and the band weights presented by gray (green) ribbons for Cu $3d_{x^2-y^2}$ and O $2p_{\sigma}$ orbitals. The Fermi level is at zero energy. Notation of the high-symmetry points: $\Gamma=(000)$, $X=(\frac{\pi}{a}00)$, $S=(\frac{\pi}{a}\frac{\pi}{a}0)$, $Z=(00\frac{\pi}{c})$, $R=(\frac{\pi}{a}0\frac{\pi}{c})$, and $A=(\frac{\pi}{a}\frac{\pi}{a}\frac{\pi}{c})$.

narrow, well separated peak at Fermi level (see Fig. 2) originates from the four antibonding Cu $3d$ -O $2p$ - σ bands according to the four Cu sites per unit cell (see Fig. 3).

In order to calculate the orbital-resolved density of states and the band characters (fat bands), we use a local coordinate system with new x and y axes running from the central copper atom of the Cu-O plaquette into the direction of the neighboring oxygen atoms. Figure 2 (middle and lower panel) demonstrates that the antibonding states at the Fermi level are generated predominantly by Cu $3d_{x^2-y^2}$ and O $2p_{\sigma}$ orbitals. The so called “fat band plot” in Fig. 3 shows in detail the dominant contribution of the Cu $3d_{x^2-y^2}$ and the O $2p_{\sigma}$ orbitals to the four well-isolated bands crossing Fermi level. The dispersions of the antibonding bands in the tetragonal plane (along Γ - X) and parallel to the tetragonal axis (along Γ - Z) show comparable width, pointing to a possibly more three-dimensional electronic structure rather than a well pronounced one-dimensional behavior.

The Bi contribution to the states at Fermi level is very small and can be neglected in good approximation. Therefore, an effective one-band model is appropriate for the description of the low-lying excitations in Bi_2CuO_4 .

For a microscopic analysis of the relevant electronic interactions, we have included 12 transfer integrals (see Fig. 4) in our tight-binding model: hopping parameters within the structural chain along the z direction to first and second neighbors as well as coupling between the structural chains up to the third neighboring chain. The tight-binding Hamiltonian for the four half-filled bands leads to a 4×4 matrix, which was solved analytically.⁴⁶ The matrix and its eigenvalues are given in Appendix A. We note that the matrix can be transformed into a block-diagonal form, which was used for the calculation of the spin wave dispersion (Sec. V).

The values for transfer integrals t_{ij} have been obtained by combination of two numerical procedures: (i) using the energy eigenvalues at high-symmetry points and (ii) a least squares fit. The difference of transfer integrals evaluated by the two procedures does not exceed 5% for the main interactions.

The resulting tight-binding fit is presented in Fig. 5, in excellent agreement with the underlying calculated LDA band structure. The small discrepancies in the lower part of the band structure (on the Γ - Z line) can be explained by the

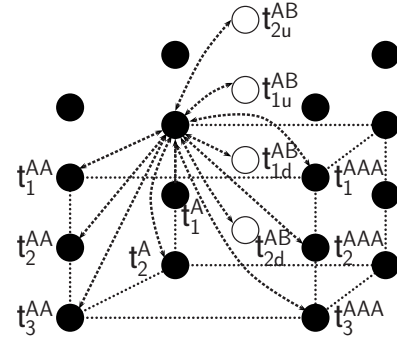


FIG. 4. The transfer integrals, involved in the tight-binding model: first (t_1^A) and second (t_2^A) in-chain neighbors, four integrals for the interactions between the neighboring chains of different sublattices (t_{1u}^{AB} , t_{1d}^{AB} , t_{2u}^{AB} , and t_{2d}^{AB}), three integrals for the interaction between the neighboring chains of the same sublattice (t_1^{AA} , t_2^{AA} , and t_3^{AA}), and three for the second-neighbor chain of the same sublattice (t_1^{AAA} , t_2^{AAA} , and t_3^{AAA}). The superscripts A and B mean sublattice, the number in the subscript means the order of neighbor, and u and d mean along the positive (up) or negative (down) c direction, respectively.

hybridization with the other orbitals for this part of the k space visible in the band weight picture (Fig. 3). Only 5 out of 12 transfer integrals appeared to have sizable values: first- and second-neighbor hopping along the z axis and three couplings between neighboring chains (see Fig. 4). The values of the leading transfer integrals are given in Table I (first row). All other transfer integrals are smaller than 10 meV.

The obtained transfer integrals allow us to estimate the exchange integrals. The total exchange consists of antiferromagnetic and ferromagnetic contributions: $J = J^{AF} + J^{FM}$. In the case of the strongly correlated limit ($U \gg t_{ij}$) which is well justified for our model, J^{AF} can be derived from an extended Hubbard model mapped to the corresponding Heisenberg model: $J_{ij}^{AF} = 4t_{ij}^2 / U_{eff}$, where t_{ij} is a transfer integral and U_{eff} is the difference of the on-site correlation U and the intersite repulsion V_{ij} . Because of the narrow bandwidth and the resulting poor screening, we adopted for our analysis typical values for the plaquette U_{eff} in the range of 4–5 eV.⁴⁷ The resulting exchange integrals are presented in Table I (rows 2 and 3). The ferromagnetic contribution to the total exchange integral is commonly caused by sharing

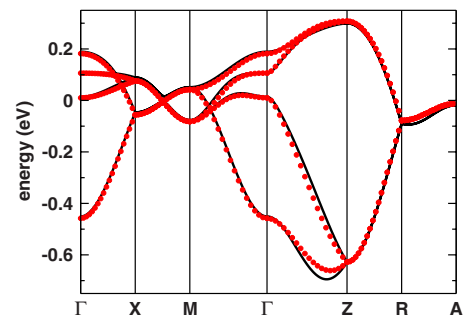


FIG. 5. (Color online) The tight-binding fit presented by gray (red) circles of the LDA band structure (black). The notation of the k points is the same as that in Fig. 3.

TABLE I. Transfer integrals (first row) and exchange integrals, derived from the tight-binding fit [second ($U_{eff}=4$ eV) and third ($U_{eff}=5$ eV) rows], LSDA+ U calculations (fourth row), spin wave dispersion (fifth row), and experimental data (following rows). All values are given in meV.

Path X	X_{1u}^{AB}	X_{2d}^{AB}	X_{1d}^{AB}	X_1^A	X_2^A
t (see Appendix A)	74	-40	36	21	-18
J (tight binding, $U_{eff}=4$ eV)	5.48	1.60	1.30	0.44	0.32
Set 1, J (tight binding, $U_{eff}=5$ eV)	4.38	1.28	1.04	0.35	0.26
J (LSDA+ U , $U_d=6.5$ eV)		$\Sigma=5.14$	0.85	0.88	
Set 2, J (spin wave dispersion)	4.7	0.44	0.85	0.88	
J , single crystal neutron diffraction ^a	0.4	4.4	1.4	1.6	
J , single crystal neutron scattering and/or diffraction ^b $\perp z$	5.86		2.06	-0.34	-0.34
J , single crystal neutron scattering and/or diffraction ^b $\parallel z$	5.68		1.72	-0.86	-1.2
J , two-magnon Raman scattering ^c	0.38	4.6	1.26	1.36	

^aReference 50.

^bReference 23.

^cReference 51.

orbitals.⁴⁸ Taking into account the absence of direct connection between the CuO_4 plaquettes, we assume that J^{FM} is small. *A posteriori*, this assumption is well justified by the consistent results of the LSDA+ U calculations (see below).

According to our results, the strongest antiferromagnetic exchange in this system is J_{1u}^{AB} (see Fig. 6) between the chains of different sublattices. In consequence, this leads to a three-dimensional magnetic character of this system, in agreement with the majority of the experimental data, although there is no general agreement at all for the assignment of the leading three-dimensional coupling from different experimental reports (see Table I and references therein).

The reported ^{63,65}Cu and ²⁰⁹Bi nuclear magnetic resonance spectroscopy⁴⁹ revealed a large influence of the Cu spins on the Bi site due to the magnetic interaction in this

compound, supporting our findings: the largest exchange interaction corresponds to the superexchange of the copper atoms which have a bismuth atom in between. In comparison, the in-chain transfer and therefore the in-chain exchange interactions are relatively small.

The excellent agreement of the calculated LDA bands and our tight-binding fit justifies the restriction to the short range couplings in our tight-binding model. Their short-range nature, especially of the magnetic couplings (see Table I), allows the independent estimation of the exchange integrals using total energy differences for different spin arrangements.

Spin-polarized calculations within the LSDA result in a splitting of spin-up and spin-down densities, but the resulting energy gap is much too small compared to spectroscopic data.²⁹ This is easy to understand because the size of the band gap is governed by the strong Coulomb correlation and not by the considerably smaller intra-atomic exchange splitting. This strong on-site correlation U_d can be taken into account within a self-consistent calculation by the LSDA+ U approximation. In order to reproduce the experimental gap, U_d was fitted to O 2p x-ray absorption spectra,²⁸ resulting in a value of $U_d \approx 6.5$ eV. This value is slightly smaller than in La_2CuO_4 , where a value of $U_d \approx 7.3$ eV was obtained by fitting the calculated exchange value⁵² to the experimentally measured value.⁵³ A possible reason is the incorrect behavior of the LSDA+ U for $U \gg t$, overestimating the suppression of the Cu-O hybridization resulting in too narrow bands and therefore overestimating the gap for a given U_d .

Thus, for an independent estimate of the short-range exchange constants, we performed LSDA+ U calculations for different spin configurations. The constructed supercells possess the same volume as the nonmagnetic unit cell and allow four different magnetic arrangements (see Fig. 7). The construction of larger supercells, including more long-range interactions, causes numerical problems with respect to convergence and to numerical accuracy, especially because of the small values for these long-range interactions following

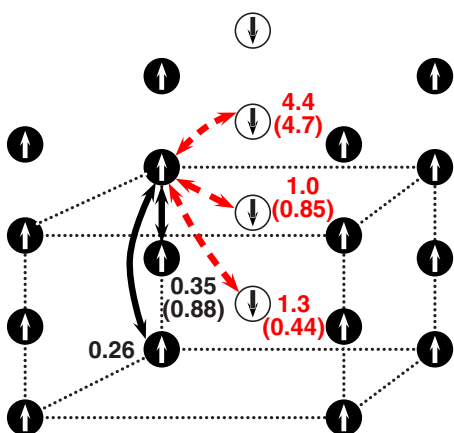


FIG. 6. (Color online) The exchange integrals, obtained by mapping the tight-binding fit of the LDA band structure to the Heisenberg model (upper value) and derived from total energy LSDA+ U calculations and spin wave dispersion (values shown in brackets). Only five physically important values are shown. The superexchange between the neighboring chains of different sublattices plays a dominant role. All values are given in meV.

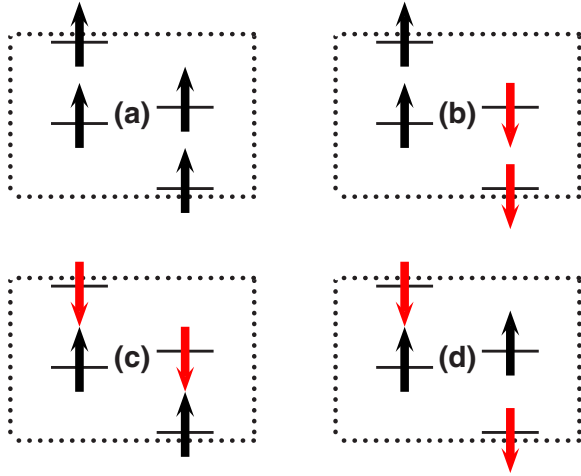


FIG. 7. (Color online) Different spin arrangements in the Bi_2CuO_4 structure computed by the LSDA+ U approach. The magnetic ground state observed by neutron diffraction (Ref. 24) is shown in the upper right panel (b).

from our tight-binding analysis presented above. Therefore, we restrict ourselves to the magnetic arrangements given in Fig. 7.

As a first result, the LSDA+ U calculations reproduce the observed magnetic ground state²⁴ [panel (b) in Fig. 7] with a minimum in the total energy. As differences between total energies of different magnetic arrangements for a system with well localized spins appear due to the spin degrees of freedom, the energies can be mapped onto the Heisenberg model:

$$\hat{H} = \sum_{\langle ij \rangle} J_{ij} \vec{S}_i \cdot \vec{S}_j. \quad (1)$$

From the four magnetic arrangements shown in Fig. 7, we can derive three exchange integrals, listed in Table I fourth row). Although only the sum of the two leading exchange interactions, $J_{1u}^{AB} + J_{1d}^{AB}$, can be calculated using the LSDA+ U for the presented spin pattern, we find a surprisingly good agreement between the LSDA+ U and the tight-binding (TB)-derived magnetic couplings. This also proves that the ferromagnetic contributions to the total exchange that are neglected in the TB-derived values are rather small.

The size of the exchange contributions from further neighbors can be independently estimated comparing the measured Curie-Weiss temperature of 96 K in Ref. 39 with the exchange constants given in Table I using the relation

$$\Theta_{CW} = \sum_i \frac{Z}{4} J_i, \quad (2)$$

where Z is the number of neighbors. This leads us to a value of 1.2 ± 0.2 meV for the *sum* of all missing (not listed in Table I) exchange interactions. This shows once more the consistency of our approach in good agreement with the most recent experimental data.^{23,51}

Regarding the widely scattering experimental reports for the exchange integrals (see Table I), our calculational results strongly favor the most recent reports from neutron

scattering²³ and two-magnon Raman scattering data.⁵¹ Because in both reports a reliable distinction of J_{1u}^{AB} and J_{2d}^{AB} was not possible, the authors mapped the sum of both parameters either completely to J_{1u}^{AB} (in Ref. 23) or mostly to J_{2d}^{AB} (in Ref. 51) based on structural arguments. From our magnetic supercell calculations using the LSDA+ U scheme, we also obtain (set 1) the sum $J_{1u}^{AB} + J_{2d}^{AB} = 5.14$ meV only. This compares extremely well with the corresponding values of 5.86 and 4.98 meV from the neutron and Raman experiments, respectively. Therefore, to distinguish between the two exchange paths, we calculate the spin wave dispersion (see Sec. V) where we fix the sum $J_{1u}^{AB} + J_{2d}^{AB} = 5.14$ meV according to our calculation and search for the best fit (set 2) using the derived spin wave dispersion (see below).

In addition, full-relativistic calculations were performed in order to determine the spin anisotropy, which is still under debate. While two-magnon Raman scattering⁵¹ and cluster calculations⁵⁴ result in an easy-axis spin alignment, the anti-ferromagnetic resonance⁵⁵ and spin-flop studies³⁹ propose easy-plane anisotropy. For the chain cuprate Li_2CuO_2 , exhibiting a very similar magnetic ground state compared to Bi_2CuO_4 , calculations including the spin-orbit coupling found an easy-axis anisotropy⁵⁶ in agreement with the experimental data.¹⁸ Therefore, we carried out calculations for the spins lying into the tetragonal plane ([001] direction) and parallel to the tetragonal axis ([001] direction). As the result, the latter one exhibits a slightly lower total energy, corresponding to an easy-axis anisotropy. This easy-axis anisotropy together with the estimated exchange constants J_{ij} is used for the calculation of the spin wave dispersion and the Néel temperature T_N presented in the following section.

V. MAGNON SPECTRUM AND NÉEL TEMPERATURE

As we have seen, the model of magnetic interactions in Bi_2CuO_4 is rather complex. Every copper ion interacts with a large number of neighbors via a lot of exchange paths. That is why the empirical modeling of various experiments may be ambiguous. For example, the spin wave dispersion⁵⁰ is well described by different sets in Refs. 50 and 51 within the frameworks of essentially the same model. In such situation, the parameter-free LSDA and LSDA+ U calculations may substantially help in establishing an adequate model. Below, we calculate the spin wave dispersion, magnetic moment, and Néel temperature for the model established in previous sections. It is given by anisotropic Heisenberg Hamiltonian

$$\hat{H} = + \frac{1}{2} \sum_{\mathbf{R}, \delta} \left[J_{\delta}^z \hat{S}_{\mathbf{R}}^z \hat{S}_{\mathbf{R}+\delta}^z + \frac{J_{\delta}^{xy}}{2} (\hat{S}_{\mathbf{R}}^+ \hat{S}_{\mathbf{R}+\delta}^- + \hat{S}_{\mathbf{R}}^- \hat{S}_{\mathbf{R}+\delta}^+) \right], \quad (3)$$

where \mathbf{R} runs over lattice sites and δ enumerates the neighbors of the \mathbf{R} th site. We have adopted the claim of Ref. 51 that the anisotropy axis is c .

Using Tyablikov decoupling scheme [random phase approximation (RPA)],^{57,58} we find the retarded Green's function (GF) (see Appendix B for the details and notations),

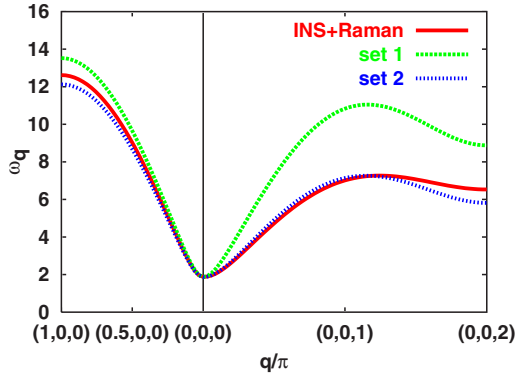


FIG. 8. (Color online) The spin wave dispersion for the model (3) given by two different sets (see Table I) compared with INS + Raman data from Ref. 51.

$$G_{AA}(\mathbf{q}, \omega) \equiv \frac{1}{N} \sum_{\mathbf{n}, \mathbf{m} \in A} e^{-i\mathbf{q}(\mathbf{n}-\mathbf{m})} \langle \langle \hat{S}_{\mathbf{n}}^+ \hat{S}_{\mathbf{m}}^- \rangle \rangle = \frac{2m(\omega + mA_{\mathbf{q}})}{\omega^2 - \omega_{\mathbf{q}}^2}, \quad (4)$$

where \mathbf{n}, \mathbf{m} run over sites of the same magnetic sublattice, $m = \langle \hat{S}_{\mathbf{n}}^z \rangle$ denotes the magnetization of sublattice A , $\omega_{\mathbf{q}} = 2m\omega_{\mathbf{q}}^{SW}$, and $\omega_{\mathbf{q}}^{SW}$ is the free spin wave dispersion [i.e., the dispersion that appears in the first order ($\sim S$) of $1/S$ expansion of Holstein-Primakoff representation of the Hamiltonian \hat{H} in Eq. (3)],

$$\omega_{\mathbf{q}}^{SW} \equiv \frac{1}{2} \sqrt{A_{\mathbf{q}}^2 - |B_{\mathbf{q}}|^2}, \quad A_{\mathbf{q}} \equiv J_{AB}^z(0) - J_A^z(0) + J_A^{xy}(\mathbf{q}), \quad (5)$$

$$B_{\mathbf{q}} \equiv J_{AB}^{xy}(\mathbf{q}),$$

$$\begin{aligned} J_{AB}^{\alpha}(\mathbf{q}) &= \sum_{\delta_{AB}} J_{\delta_{AB}}^{\alpha} e^{i\mathbf{q}\delta_{AB}} \\ &= 4 \cos \frac{q_x a}{2} \cos \frac{q_y a}{2} \exp(-2i q_z z_{cu}) \\ &\quad \times \left\{ \left[J_{1d} + (J_{1u} + J_{2d}) \cos \frac{q_z c}{2} + J_{2u} \cos q_z c \right] \right. \\ &\quad \left. + i \left[(J_{1u} - J_{2d}) \sin \frac{q_z c}{2} + J_{2u} \sin q_z c \right] \right\}, \\ J_A^{\alpha}(\mathbf{q}) &= \sum_{\delta_A} J_{\delta_A}^{\alpha} e^{i\mathbf{q}\delta_A} = 2J_{1A} \cos \frac{q_z c}{2} + 2J_{2A} \cos q_z c. \end{aligned} \quad (6)$$

Here, $\alpha = z, xy$. The peculiarity of the Bi_2CuO_4 structure results in the complexity of $J_{AB}^{\alpha}(\mathbf{q}) = J_{BA}^{\alpha*}(\mathbf{q})$.

It is well known that the RPA overestimates the spin wave energy renormalization at zero temperature.^{59,60} Thus, the inelastic neutron scattering (INS) experiment results should be compared with $\omega_{\mathbf{q}}^{SW}$ rather than with $\omega_{\mathbf{q}}$.

Figure 8 shows the comparison of the dispersions [Eq. (5)] with the model of Ref. 51 which fits both INS and Raman scattering data simultaneously. Our model [Eq. (5)] is

supplemented with the anisotropy $D = A_0 - B_0$. The chosen value of the anisotropy $D = \sqrt{4\Delta_{\text{exp}}^2 - B_0^2} - B_0$ reproduces the experimental value of the gap in the spin wave spectrum $\Delta_{\text{exp}} \approx 1.87$ meV.

We have used two sets of exchange parameters (see Table I). The first set (set 1, row 3 in Table I) is obtained from the effective Hubbard model having one-particle hoppings taken from our tight-binding fit of the LDA band structure. We have chosen the effective Hubbard U value to be $U = 5$ eV. This set qualitatively reproduces the results of INS, but it overestimates the spin wave dispersion. Let us recall that effective Hubbard model provides only antiferromagnetic contribution to the superexchange as we have discussed in the previous section.

Better agreement may be achieved with a semiempirical set (set 2, row 5 in Table I). It contains four exchange constants. The values $J_{1u} + J_{2d}$, J_{1d} , and J_{1A} are taken from LSDA+ U calculation. This results in $J_{1u} = 4.7$ meV and $J_{2d} = 0.44$ meV for the best fit to the INS²³ and Raman data.⁵¹ Obtaining $J_{1u} = 4.7$ meV as the leading exchange term this way is also in good agreement with the result from the TB mapping procedure with $J_{1u} = 4.38 - 5.48$ meV (see Table I).

When $J_{2u} = 0$, the exchange constants J_{1u} and J_{2d} enter symmetrically in the $\omega_{\mathbf{q}}^{SW}$ expression [Eqs. (5) and (6)]. In this case, only the square of the value $\Delta J = J_{1u} - J_{2d}$ enters Eq. (5). The values ($J_{1u} = 4.7$ meV and $J_{2d} = 0.44$ meV) mentioned above are obtained by fixing the ratio J_{1u}/J_{2d} according to the tight-binding fit. So, it is not surprising that our set 2 gives a dispersion close to the experimentally observed one. Its main difference from the empirical set of Ref. 51 is the sign of ΔJ . The true sign of ΔJ may be established only in the model with $J_{2u} \neq 0$. The accurate analysis of the spin wave dispersion along the z direction that could provide the value of J_{2u} together with the sign of ΔJ demands very precise INS measurements. Let us mention that this dispersion is also affected by J_{2A} and other intrasublattice exchange couplings that complicate the analysis even more.

Within the standard RPA approach,^{57,58} we have calculated the Néel temperature T_N using the obtained GF [Eq. (4)]. In analogy with Ref. 60 (see also Appendix B), T_N is given by

$$T_N = \frac{1}{4 \sum_{\mathbf{q}} \frac{A_{\mathbf{q}}}{A_{\mathbf{q}}^2 - |B_{\mathbf{q}}|^2}}. \quad (7)$$

Substituting the exchange couplings from different sets into Eqs. (6) and (7), we have $T_{N, \text{Ref. 51}} \approx 47$ K, $T_{N,1} \approx 59$ K, and $T_{N,2} \approx 47$ K in surprisingly good agreement with the experimental value of $T_{N, \text{exp}} = 42 - 46$ K.

VI. SUMMARY

In this paper, the electronic and magnetic structure of Bi_2CuO_4 was investigated in a detailed, microscopic analysis. Here, we combined density functional calculations (LDA and LSDA+ U), a tight-binding model of the nonmagnetic band structure with a subsequent mapping onto a Heisenberg model, and calculations of the magnetic anisotropy, the spin

wave dispersion, and the Néel temperature using the exchange integrals obtained this way. Our results clearly favor the interpretation of recent neutron scattering²³ and Raman data.⁵¹ In addition, we could identify the leading coupling unambiguously. Our main conclusions are as follows: (i) Bi_2CuO_4 is a compound with a rather three-dimensional electronic and magnetic structure. Therefore, quantum fluctuations should be strongly suppressed. This is also reflected in the comparably large ordered magnetic moment and a Néel temperature comparable with the leading exchange term. (ii) The main coupling is an antiferromagnetic superexchange between neighboring chains. (iii) The coupling along the structural chains is relatively weak. (iv) The ferromagnetic arrangement along the chains originates from the zigzaglike antiferromagnetic interchain coupling. (v) The compound exhibits an easy-axis anisotropy.

ACKNOWLEDGMENTS

We thank M. Knupfer for the communication of the O 2p x-ray absorption data. We appreciate fruitful discussions with J. Málek, M. D. Johannes, K. Koepernik, U. Nitzsche, and Yu. Grin. The DFG (436/UKR/17/8/05, R.O.K.; Emmy-Noether program, O.J. and H.R.) and the GIF (1-811-237.14103) are acknowledged for financial support. We kindly acknowledge the use of the supercomputing facilities at ZIH Dresden.

APPENDIX A: TIGHT-BINDING MODEL

The tight-binding model presented in Sec. IV leads to a 4×4 matrix according to the four antibonding Cu-O states originating from the four Cu sites per unit cell. This matrix is given by

$$\begin{pmatrix} \alpha & \beta & \chi + \varphi & \zeta + \xi \\ \beta & \alpha & \zeta + \xi & \chi + \varphi \\ \chi^* + \varphi^* & \zeta^* + \xi^* & \alpha & \beta \\ \zeta^* + \xi^* & \chi^* + \varphi^* & \beta & \alpha \end{pmatrix}, \quad (\text{A1})$$

with

$$\alpha = \varepsilon_0 - 2t_2^A \cos(k_z c) - 2t_1^{AA} [\cos(k_x a) + \cos(k_y a)], \quad (\text{A2})$$

$$\beta = -2t_1^A \cos\left(k_z \frac{c}{2}\right) - 2t_2^{AA} [\cos(k_x a) + \cos(k_y a)] \cos\left(k_z \frac{c}{2}\right), \quad (\text{A3})$$

$$\chi = -4t_{1d}^{AB} \cos\left(k_x \frac{a}{2}\right) \cos\left(k_y \frac{a}{2}\right) \exp[-k_z(0.15c)], \quad (\text{A4})$$

$$\varphi = -4t_{2u}^{AB} \cos\left(k_x \frac{a}{2}\right) \cos\left(k_y \frac{a}{2}\right) \exp[k_z(0.85c)], \quad (\text{A5})$$

$$\zeta = -4t_{1u}^{AB} \cos\left(k_x \frac{a}{2}\right) \cos\left(k_y \frac{a}{2}\right) \exp[k_z(0.35c)], \quad (\text{A6})$$

$$\xi = -4t_{2d}^{AB} \cos\left(k_x \frac{a}{2}\right) \cos\left(k_y \frac{a}{2}\right) \exp[-k_z(0.65c)], \quad (\text{A7})$$

where a and c are lattice constants and k_x, k_y, k_z is a vector in reciprocal lattice (the notation for transfer integrals is given on Fig. 4). The four eigenvalues of this matrix are the following:

$$\alpha - \beta \pm \sqrt{(\chi + \varphi - \xi - \zeta)(\chi^* + \varphi^* - \xi^* - \zeta^*)}, \quad (\text{A8})$$

$$\alpha + \beta \pm \sqrt{(\chi + \varphi - \xi - \zeta)(\chi^* + \varphi^* + \xi^* + \zeta^*)}. \quad (\text{A9})$$

APPENDIX B: TEMPERATURE DEPENDENT RETARDED GREEN'S FUNCTION

Here, we give the details of analytical calculations that have led us to Eqs. (4), (5), and (7).

As it was mentioned above, the unit cell of tight-binding model contains two sites with the vector radii $\rho_A = (3/4, 1/4, 1/2 - z_{cu})$, and $\rho_B = (1/4, 3/4, 1/2 + z_{cu})$. So, the unit cell is two times smaller than the chemical cell and has the dimensions $(a, a, c/2)$. The unit cell of magnetic structure coincides with that of tight-binding model. Thus, the magnetic Brillouin zone is a rectangular box, $-\pi/a < q_x, q_y < \pi/a, -2\pi/c < q_z < 2\pi/c$.

We will calculate the retarded Green's function

$$\begin{aligned} G_{s_1 s_2}(\mathbf{q}, \omega) &= -i \int_{t'}^{\infty} dt e^{i\omega(t-t')} \langle [\hat{S}_{-\mathbf{q}s_1}^+(t), \hat{S}_{\mathbf{q}s_2}^-(t')] \rangle \\ &\equiv \langle \langle \hat{S}_{-\mathbf{q}s_1}^+ | \hat{S}_{\mathbf{q}s_2}^- \rangle \rangle, \end{aligned} \quad (\text{B1})$$

where

$$\hat{S}_{\mathbf{q}s}^{\alpha} = \frac{1}{\sqrt{N}} \sum_{\mathbf{n} \in s} e^{i\mathbf{q}(\mathbf{n}+\rho_s)} \hat{S}_{\mathbf{n}+\rho_s}^{\alpha}, \quad (\text{B2})$$

$\alpha = +, -, z$ and $s = A, B$ define the sublattice, and \mathbf{n} enumerates the sites of the Bravais lattice of magnetic structure, i.e., the sum goes over the sites of one sublattice. N is the total number of *unit cells* that coincides with the number of sites in a sublattice. The $[\dots, \dots]$ means the commutator. The expectation value denotes the thermal average:

$$\langle \dots \rangle = Q^{-1} \text{Sp}[e^{-\beta \hat{H}} \dots], \quad Q = \text{Sp}e^{-\beta \hat{H}}. \quad (\text{B3})$$

Here, Sp implies taking the trace of an operator and $\beta = (k_B T)^{-1}$ is an inverse temperature. The time dependence of an operator $\hat{X}(t)$ is given by $\hat{X}(t) = e^{it\hat{H}} \hat{X} e^{-it\hat{H}}$.

The equation of motion for GF [Eq. (B1)] gives

$$\begin{aligned} \omega G_{AA}(\mathbf{q}, \omega) &= \langle [\hat{S}_{-\mathbf{q}A}^+, \hat{S}_{\mathbf{q}A}^-] \rangle + \langle \langle [\hat{S}_{-\mathbf{q}A}^+, \hat{H}] \hat{S}_{\mathbf{q}A}^- \rangle \rangle \\ &= 2m_A + \frac{1}{\sqrt{N}} \sum_{\mathbf{n} \in A} e^{-i\mathbf{q}(\mathbf{n}+\rho_A)} \sum_{\delta} \langle \langle -J_{\delta}^z \hat{S}_{\mathbf{n}+\rho_A}^+ \hat{S}_{\mathbf{n}+\rho_A+\delta}^z \\ &\quad + J_{\delta}^{xy} \hat{S}_{\mathbf{n}+\rho_A}^z \hat{S}_{\mathbf{n}+\rho_A+\delta}^+ | \hat{S}_{\mathbf{q}A}^- \rangle \rangle. \end{aligned} \quad (\text{B4})$$

Here, $m_A = \langle \hat{S}_{\mathbf{n}+\rho_A}^z \rangle \equiv m$ denotes A sublattice magnetization.

According to experimental findings, we assume that the magnetization of sublattice B is $m_B = -m_A$.

The RPA decoupling^{57,58} of higher order GF substitutes

$$\langle\langle \hat{S}_n^+ \hat{S}_m^z | \hat{S}_{qA}^- \rangle\rangle \approx \langle \hat{S}_m^z \rangle \langle\langle \hat{S}_n^+ | \hat{S}_{qA}^- \rangle\rangle. \quad (\text{B5})$$

Then, we find

$$(\omega - mA_q)G_{AA}(\mathbf{q}, \omega) = 2m + mB_q G_{BA}(\mathbf{q}, \omega),$$

$$(\omega + mA_q)G_{BA}(\mathbf{q}, \omega) = -mB_q^* G_{AA}(\mathbf{q}, \omega). \quad (\text{B6})$$

The solution of the system in Eq. (B6) gives Eq. (4).

Let us now calculate the Néel temperature. The additional equation for the value of the sublattice magnetization is given by

$$\frac{1}{2} - m = \frac{1}{N} \sum_{\mathbf{q}} \langle \hat{S}_{qA}^- \hat{S}_{-qA}^+ \rangle, \quad (\text{B7})$$

where the correlation function $\langle \hat{S}_{qA}^- \hat{S}_{-qA}^+ \rangle$ is related with GF,

$$\begin{aligned} \langle \hat{S}_{qA}^- \hat{S}_{-qA}^+ \rangle &= \int_{-\infty}^{+\infty} \frac{d\omega}{e^{\beta\omega} - 1} \left[-\frac{1}{\pi} \text{Im} G_{AA}(\mathbf{q}, \omega) \right] \\ &= m \left(\frac{A_q}{\sqrt{A_q^2 - |B_q|^2}} \coth \frac{\beta\omega_q}{2} - 1 \right). \end{aligned} \quad (\text{B8})$$

Equations (B7) and (B8) close the RPA self-consistency loop and give the equation for the temperature dependent sublattice magnetization,

$$\frac{1}{2} = m \frac{1}{N} \sum_{\mathbf{q}} \frac{A_q}{\sqrt{A_q^2 - |B_q|^2}} \coth \frac{\beta\omega_q}{2}. \quad (\text{B9})$$

For zero temperature, we have $\coth \frac{\beta\omega_q}{2} \rightarrow 1$, which gives

$$m(T=0) = \langle \hat{S}_A^z \rangle = \frac{1}{\frac{2}{N} \sum_{\mathbf{q}} \frac{A_q}{\sqrt{A_q^2 - |B_q|^2}}}. \quad (\text{B10})$$

Substituting the values for exchange integrals, we have $m_1(0) \approx 0.45$ for set 1, $m_2(0) \approx 0.43$ for set 2, and $m_{\text{Ref.51}}(0) = 0.44$ for the set of Ref. 51.

In the vicinity of the Néel temperature, $m \rightarrow 0$ then $\coth \frac{\beta\omega_q}{2} \approx 2T/\omega_q$. This gives for the Néel temperature the estimate in Eq. (7).

*rosner@cpfs.mpg.de

- ¹H. Bethe, *Z. Phys.* **71**, 205 (1931).
- ²J. C. Bonner and M. E. Fisher, *Phys. Rev.* **135**, A640 (1964).
- ³H. J. Schulz, *Phys. Rev. Lett.* **77**, 2790 (1996).
- ⁴I. Affleck, M. Gelfand, and R. R. P. Singh, *J. Phys. A* **27**, 7313 (1994); **28**, 1787(E) (1995).
- ⁵Z. Wang, *Phys. Rev. Lett.* **78**, 126 (1997).
- ⁶K. M. Kojima *et al.*, *Phys. Rev. Lett.* **78**, 1787 (1997).
- ⁷H. Rosner, H. Eschrig, R. Hayn, S.-L. Drechsler, and J. Málek, *Phys. Rev. B* **56**, 3402 (1997).
- ⁸M. Enderle *et al.*, *Europhys. Lett.* **70**, 237 (2005).
- ⁹L. Capogna, M. Mayr, P. Horsch, M. Raichle, R. K. Kremer, M. Sofin, A. Maljuk, M. Jansen, and B. Keimer, *Phys. Rev. B* **71**, 140402(R) (2005).
- ¹⁰S.-L. Drechsler, J. Richter, A. A. Gippius, A. Vasiliev, A. A. Bush, A. S. Moskvina, J. Málek, Y. Prots, W. Schnelle, and H. Rosner, *Europhys. Lett.* **73**, 83 (2006).
- ¹¹A. A. Gippius, E. N. Morozova, A. S. Moskvina, A. V. Zalesky, A. A. Bush, M. Baenitz, H. Rosner, and S.-L. Drechsler, *Phys. Rev. B* **70**, 020406(R) (2004).
- ¹²T. Masuda, A. Zheludev, A. Bush, M. Markina, and A. Vasiliev, *Phys. Rev. Lett.* **92**, 177201 (2004).
- ¹³S.-L. Drechsler, J. Málek, J. Richter, A. S. Moskvina, A. A. Gippius, and H. Rosner, *Phys. Rev. Lett.* **94**, 039705 (2005).
- ¹⁴T. Masuda, A. Zheludev, A. Bush, M. Markina, and A. Vasiliev, *Phys. Rev. Lett.* **94**, 039706 (2005).
- ¹⁵S. Park, Y. J. Choi, C. L. Zhang, and S.-W. Cheong, *Phys. Rev. Lett.* **98**, 057601 (2007).
- ¹⁶S.-L. Drechsler, O. Volkova, A. N. Vasiliev, N. Tristan, J. Richter, M. Schmitt, H. Rosner, J. Málek, R. Klingeler, A. A. Zvyagin, and B. Büchner, *Phys. Rev. Lett.* **98**, 077202 (2007).
- ¹⁷K. Sreedhar, P. Ganguly, and S. Ramasesha, *J. Phys. C* **21**, 1129 (1988).
- ¹⁸M. Boehm, S. Coad, B. Roessli, A. Zheludev, M. Zolliker, P. Böni, D. M. Paul, H. Eisaki, N. Motoyama, and S. Uchida, *Europhys. Lett.* **43**, 77 (1998).
- ¹⁹R. Weht and W. E. Pickett, *Phys. Rev. Lett.* **81**, 2502 (1998).
- ²⁰Y. Mizuno, T. Tohyama, and S. Maekawa, *Phys. Rev. B* **60**, 6230 (1999).
- ²¹R. Neudert *et al.*, *Physica C* **317-318**, 312 (1999).
- ²²S.-L. Drechsler, J. Richter, J. Málek, A. S. Moskvina, R. Klingeler, and H. Rosner, *J. Magn. Magn. Mater.* **290-291**, 345 (2005).
- ²³B. Roessli, P. Fischer, A. Furrer, G. Petrakovskii, K. Sabina, V. Valkov, and B. Fedoseev, *J. Appl. Phys.* **73**, 6448 (1993).
- ²⁴J. L. García-Muñoz, J. Rodríguez-Carvajal, F. Sapiña, M. J. Sanchez, R. Ibáñez, and D. Beltrán-Porter, *J. Phys.: Condens. Matter* **2**, 2205 (1990).
- ²⁵R. Troć, J. Janicky, I. Filatow, P. Fischer, and A. Murasik, *J. Phys.: Condens. Matter* **2**, 6989 (1990).
- ²⁶G. A. Petrakovskii, K. A. Sablina, A. I. Pankrats, V. M. Vorotinov, A. Furrer, B. Roessli, and P. Fischer, *J. Magn. Magn. Mater.* **140-144**, 1991 (1995).
- ²⁷Z. V. Popović, G. Kliche, M. J. Konstantinović, and A. Revcolevschi, *J. Phys.: Condens. Matter* **4**, 10085 (1992).
- ²⁸M. Knupfer (private communication).
- ²⁹A. Goldoni, U. del Pennino, F. Parmigiani, L. Sangaletti, and A. Revcolevschi, *Phys. Rev. B* **50**, 10435 (1994).
- ³⁰A. Goldoni, U. del Pennino, F. Parmigiani, L. Sangaletti, and A. Revcolevschi, *Solid State Commun.* **90**, 161 (1994b).
- ³¹W. E. Pickett, *Phys. Rev. Lett.* **79**, 1746 (1997).
- ³²R. Valentí, T. Saha-Dasgupta, C. Gros, and H. Rosner, *Phys. Rev. B* **67**, 245110 (2003).

- ³³T. Saha-Dasgupta, R. Valentí, H. Rosner, and C. Gros, *Europhys. Lett.* **67**, 63 (2004).
- ³⁴H. Rosner, R. R. P. Singh, W. H. Zheng, J. Oitmaa, S.-L. Drechsler, and W. E. Pickett, *Phys. Rev. Lett.* **88**, 186405 (2002).
- ³⁵V. R. Arpe and H. Müller-Buschbaum, *Z. Anorg. Allg. Chem.* **426**, 1 (1976).
- ³⁶J. C. Boivin, J. Trehoux, and D. Thomas, *Bull. Soc. Fr. Mineral. Cristallogr.* **99**, 193 (1976).
- ³⁷J. P. Attfield, *J. Phys.: Condens. Matter* **1**, 7045 (1989).
- ³⁸E. W. Ong, G. H. Kwei, R. A. Robinson, B. L. Ramakrishna, and R. B. Von Dreele, *Phys. Rev. B* **42**, 4255 (1990).
- ³⁹K. Yamada *et al.*, *J. Phys. Soc. Jpn.* **60**, 2406 (1991).
- ⁴⁰J. Konstantinovic, G. Stanisic, M. Ain, and G. Parete, *J. Phys.: Condens. Matter* **3**, 381 (1991).
- ⁴¹This can be explained as follows: Experiments reveal antiferromagnetic order described by ferromagnetic in-chain spin arrangement and chains antiferromagnetically arranged with respect to each other. The chains are running along the c axis; therefore, two neighboring copper atoms with $c/2$ interatomic distance have the same spin orientation. Glide planes c (space group $P4/ncc$) that run through copper atoms reflect the atoms (which has no influence on copper atoms) and translate them by $c/2$. If this glide plane would have change the spin, i.e., in the case of a c' glide plane (space group $P4/n'c'c'$), the in-chain antiferromagnetic order would have appeared, leading to the contradiction with observed magnetic order.
- ⁴²V. Koptsik, *Shubnikov's Groups* (Izdatel'stvo Moskovskogo Universiteta, Moscow, 1966).
- ⁴³K. Koepnik and H. Eschrig, *Phys. Rev. B* **59**, 1743 (1999).
- ⁴⁴J. P. Perdew and Y. Wang, *Phys. Rev. B* **45**, 13244 (1992).
- ⁴⁵H. Eschrig, K. Koepnik, and I. Chaplygin, *J. Solid State Chem.* **176**, 482 (2003).
- ⁴⁶MATHEMATICA 5.0 was used for the analytic diagonalization.
- ⁴⁷M. D. Johannes, J. Richter, S.-L. Drechsler, and H. Rosner, *Phys. Rev. B* **74**, 174435 (2006).
- ⁴⁸J. B. Goodenough, *Magnetism and the Chemical Bond* (Interscience, New York, 1976).
- ⁴⁹A. A. Gippius, A. N. Vasil'ev, G. A. Petrakovskii, A. V. Zalessky, W. Hoffmann, K. Lüders, G. Dhalenne, and A. Revcolevschi, *J. Magn. Magn. Mater.* **184**, 358 (1998).
- ⁵⁰M. Aïn, G. Dhalenne, O. Guiselin, B. Hennion, and A. Revcolevschi, *Phys. Rev. B* **47**, 8167 (1993). We have multiplied the values of the exchange integrals by a factor of 2 due to the possible misprint in the Hamiltonian.
- ⁵¹M. J. Konstantinović, Z. Konstantinović, and Z. V. Popović, *Phys. Rev. B* **54**, 68 (1996).
- ⁵²U. Nitzsche, S.-L. Drechsler, and H. Rosner (unpublished).
- ⁵³P. E. Sulewski, P. A. Fleury, K. B. Lyons, S.-W. Cheong, and Z. Fisk, *Phys. Rev. B* **41**, 225 (1990).
- ⁵⁴N. Tanaka, Y. Hirota, T. Kawakami, and K. Motizuki, *J. Magn. Magn. Mater.* **177–181**, 1387 (1998).
- ⁵⁵A. I. Pankrats, D. Y. Sobyenin, A. M. Vorotinov, and G. A. Petrakovskii, *Solid State Commun.* **109**, 263 (1999).
- ⁵⁶D. Mertz, R. Hayn, I. Opahle, and H. Rosner, *Phys. Rev. B* **72**, 085133 (2005).
- ⁵⁷S. V. Tyablikov, *Ukr. Mat. Zh.* **11**, 287 (1961).
- ⁵⁸S. V. Tyablikov, *Methods in the Quantum Theory of Magnetism* (Plenum, New York, 1967).
- ⁵⁹T. Oguchi, *Phys. Rev.* **117**, 117 (1960).
- ⁶⁰F. B. Anderson and H. B. Callen, *Phys. Rev.* **136**, A1068 (1964).